On the nature and origin of dicationic, charge-separated species formed in liquid water on X-ray irradiation

Stephan Thürmer[1], Milan Ončák[2], Niklas Ottosson[3], Robert Seidel[4], Uwe Hergenhahn[5], Stephen E. Bradforth[4], Petr Slavíček[2]* and Bernd Winter[1]*

To understand the yield and patterns of damage in aqueous condensed matter, including biological systems, it is essential to identify the initial products subsequent to the interaction of high-energy radiation with liquid water. Until now, the observation of several fast reactions induced by energetic particles in water was not possible on their characteristic timescales. Therefore, some of the reaction intermediates involved, particularly those that require nuclear motion, were not considered when describing radiation chemistry. Here, through a combined experimental and theoretical study, we elucidate the ultrafast proton dynamics in the first few femtoseconds after X-ray core-level ionization of liquid water. We show through isotope analysis of the Auger spectra that proton-transfer dynamics occur on the same timescale as electron autoionization. Proton transfer leads to the formation of a Zundel-type intermediate $[HO^{*}\cdots H\cdots H_2O]^{+}$, which further ionizes to form a so-far unnoticed type of dicationic charge-separated species with high internal energy. We call the process proton-transfer mediated charge separation.

The primary processes in water initiated by X-rays are understood poorly despite their paramount importance in different fields. Understanding the energy and charge re-distribution on X-ray photon absorption in water is vital for the design of more-efficient radiooncology schemes[1,2], for disentangling the physical basis of genotoxic effects on living tissues[3–5], for minimizing the damage of biological samples during X-ray diffraction experiments[6] and for controlling the performance of nuclear reactors under operating conditions[7]. The current understanding of electron-initiated processes in aqueous systems after energy deposition, and the subsequent radical chemistry, was reviewed recently[8]. An explicit consideration of radicals and molecular species formed via multiple ionization processes of water, which involve, for instance, atomic oxygen and hydrogen peroxide, can be found in the radiolysis literature, for example in Hatano *et al.*[7] and Meesungnoen *et al.*[9]. However, the ultrafast processes and mechanisms in water radiolysis remain, to a large extent, unexplored.

In the present work we focus on the processes that follow oxygen 1*s* (O1*s*) core-level ionization of water. The highly excited species formed by the core ionization relaxes primarily via Auger-electron decay. As shown in Fig. 1b, Auger decay of a water molecule involves refilling the water-core hole by one of the valence electrons, and the simultaneous emission of another valence electron, the Auger electron, from the same water molecule. The resulting highly reactive doubly ionized $H_2O^{2+}_{(aq)}$ molecule, with both vacancies (holes) located at the same site (denoted here as the two-hole (2h) state), then undergoes an ultrafast Coulombic explosion to form dominantly $O + 2H^{+}$ (refs 10,11).

In recent years a set of novel non-local autoionization processes was identified to play an important role in weakly bonded atomic and molecular systems[12–14]. One such relaxation process is intermolecular Coulombic decay (ICD), initially observed on inner-valence ionization of van der Waals-bonded clusters[12,15–17] and later also in (hydrogen-bonded) water clusters[18]. In the ICD process, the energy provided by an outer valence electron on filling the vacancy is used to expel a second electron from an atom or molecule neighbouring the initially ionized site. Throughout the process the two units (two water molecules in our case) can be considered as being electronically distinct (see Fig. 1c). The final product is a doubly charged species, but with the two positive charges located on different water units, that is a $[H_2O^{+}\cdots H_2O^{+}]_{(aq)}$ complex is formed. Computational work suggests that the ICD process is a rather general mechanism for electronic deactivation in hydrogen-bonded molecules in water, such as hydrated biomolecules[19], ammonia[20,21] or water molecules that interact with a protein residue[21]. More recently, ICD-like processes were also observed for core ionization and core excitation of aqueous solutions[20,22–26]. The core-ionization induced processes of ICD type were also observed and thoroughly discussed for water[27,28] and ammonia clusters[29]. An important difference between the relaxation of core holes and of inner-valence holes is that single core-ionization energies are greater than the lowest valence double-ionization energies; thus, the Auger channel is always open on core ionization, whereas it might be energetically forbidden on inner-valence ionization[14].

Here we explore yet another alternative relaxation route of core-ionized liquid water that is mediated by the ultrafast motion of a proton in the intermediate core-hole state (summarized in Fig. 1d). The term 'mediated' and the corresponding acronym 'PTM' (proton-transfer mediated') account for the fact that some

[1]Helmholtz-Zentrum Berlin für Materialien und Energie, and Berlin Electron Storage Ring Society for Synchrotron Radiation (BESSY), 12489 Berlin, Germany, [2]Department of Physical Chemistry, Institute of Chemical Technology, Technická 5, 16628 Prague, Czech Republic, [3]FOM Institute AMOLF, Science Park 102, 1098 XG Amsterdam, The Netherlands, [4]Department of Chemistry, University of Southern California, Los Angeles, California 90089, USA, [5]Max Planck Institute for Plasma Physics, EURATOM Association, Wendelsteinstrasse 1, 17491 Greifswald, Germany.
*e-mail: petr.slavicek@vscht.cz; bernd.winter@helmholtz-berlin.de

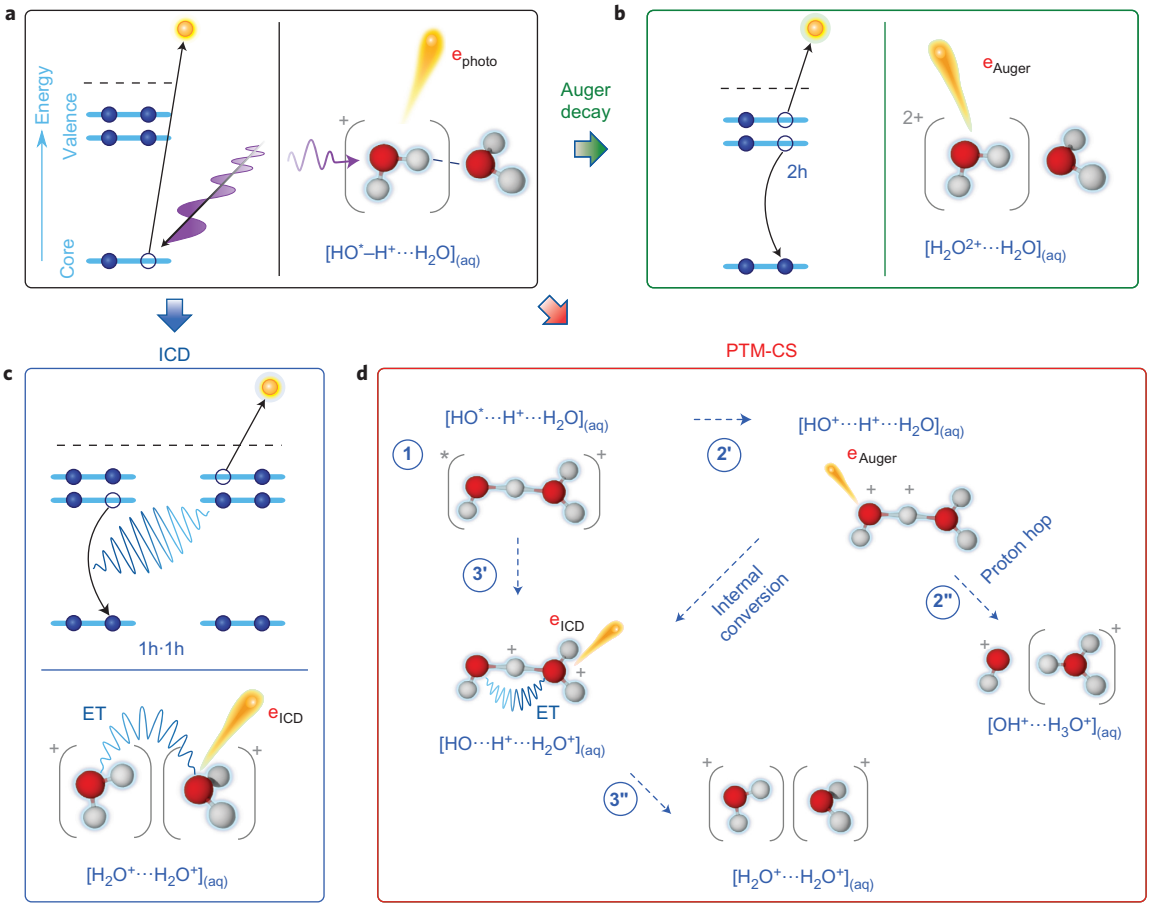

Figure 1 | Schematic of the three autoionization mechanisms of core-ionized liquid water considered here. a, The starting point is the creation of a hole in the water core-level by photoionization. Here HO* denotes the core-excited neutral species. **b**–**d**, Normal Auger decay (**b**), ICD (**c**) and PTM-CS (with the two autoionization routes of the Zundel-like intermediate) (**d**). For **b** and **c** the relevant energy levels are shown. Energy levels for **d** depend on the nuclear geometry, which varies with time during the proton-transfer process.

of the processes considered here are possible only if proton transfer takes place. These processes occur on the timescale of the O1*s* core-hole lifetime (approximately 4 fs)[30], which is comparable to the 9 fs period of a full O–H vibration in water. Experimentally, we performed a so-called core-hole clock measurement[31–33], where we detect energies of electrons emitted by autoionization from the geometrically evolving manifold of core-ionized structures. The relaxation into two-hole final states is taken to be monoexponential; the time constant is the core-hole lifetime. The Auger spectra of water thus contain temporal information about changes in the electronic structure induced by ultrafast proton transfer in the core-ionized state.

At some point during the proton transfer, the two initially interacting water units form a Zundel-type cationic species, $[HO^*\cdots H\cdots H_2O]^+_{(aq)}$ (step 1 in Fig. 1d). Relaxation by autoionization of the core-hole state can therefore take place from a continuum of non-equilibrium structures, even at this short timescale. In the proton-transfer mediated Auger (PTM-Auger) process core-excited HO* emits an Auger electron (branch to the right in Fig. 1d). In the proton-transfer mediated ICD process (PTM-ICD) energy released in the core refill of HO* is, instead, used to ionize the H_2O of the Zundel-type species (downwards branch in Fig. 1d). Both mechanisms are written explicitly in Fig. 1d, with steps 2′ and 2″, and steps 3′ and 3″ for the Auger and ICD cases, respectively. Here, internal conversion may occur because the states formed in the upper process have somewhat larger energy, as we show below.

We denote the final electronic states of these charge-separated dicationic complexes, $[HO^+\cdots H_3O^+]_{(aq)}$ and $[H_2O^+\cdots H_2O^+]_{(aq)}$, as 1h·1h (as opposed to 2h for normal Auger, which occurs in a ground-state geometry). We further distinguish the 1h·1h states depending on whether charge delocalization occurs through normal ICD, that is in the ground-state structure (denoted here as $(1h{\cdot}1h)_{ICD}$, see Fig. 1c), via ICD in the distorted geometry $((1h{\cdot}1h)_{ICD^*}$ through PTM-ICD, see Fig. 1d, step 3′), or via local de-excitation in the distorted geometry $((1h{\cdot}1h)_{Auger}$ through PTM-Auger, see Fig. 1d, step 2′). The 1h·1h states can be distinguished experimentally from the 2h states by their different Auger electron spectra. The actual occurrence of PTM charge-separation (PTM-CS) effects is reflected in the larger intensities of the 1h·1h signature in the Auger spectra from $H_2O_{(aq)}$ than from $D_2O_{(aq)}$, as demonstrated below. The importance of nuclear dynamics for core-ionized liquid water and for water excited into the antibonding $4a_1$ state was also invoked to explain the X-ray emission spectra from liquid water[34–39]. With Auger-electron spectroscopy we now address explicitly the electronic structure of the excited intermediates and the character of the 2h final states by specifically measuring the kinetic energy (KE) of electrons emitted during nuclear relaxation. The charge-separation mechanisms (Fig. 1d) are interpreted with the help of *ab initio* calculations.

Results and discussion

Core-level ionization-induced autoionization spectra: $H_2O_{(aq)}$ versus $D_2O_{(aq)}$. Experimental electron-energy spectra for the

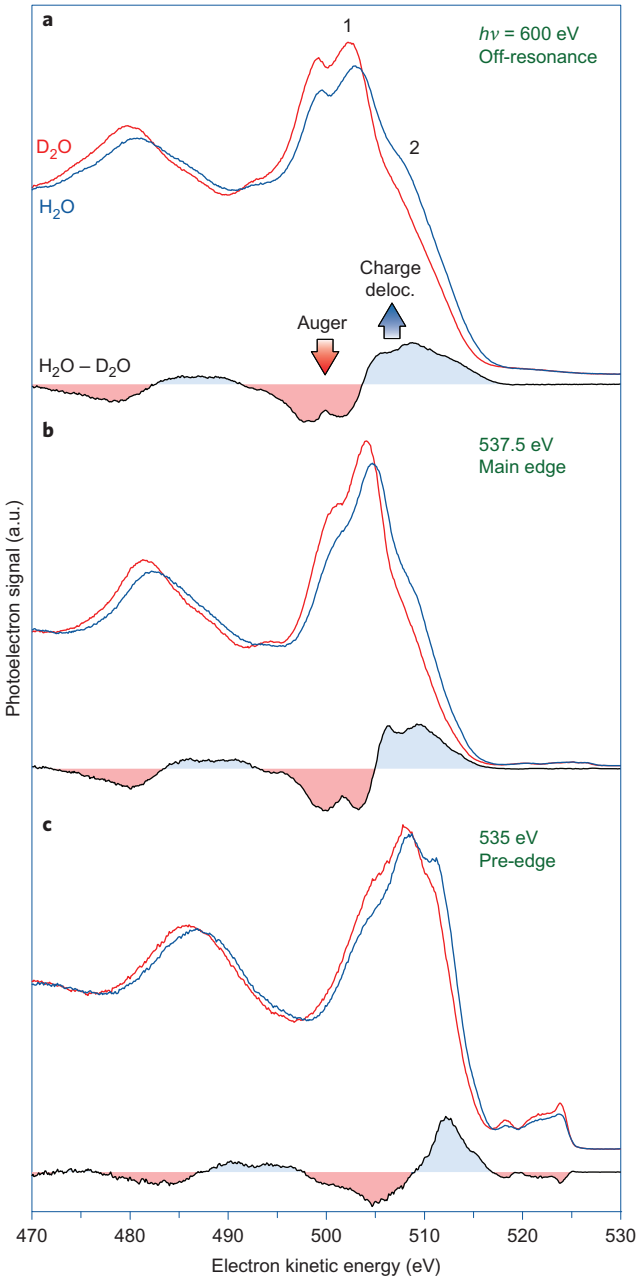

Figure 2 | Auger-electron spectra from normal (blue) and heavy (red) liquid water, together with the absolute intensity difference between the two spectra (black). a–c, Water O1*s* ionization (**a**), and main-edge (**b**) and pre-edge (**c**) excitation with photon energies as indicated. All spectra are corrected for photon flux, yielding integrated signal areas of the H_2O traces that differ by less than 5% of the respective D_2O traces. For ionization (**a**), the positive difference signal (blue area) identifies non-local final states (charge delocalization (deloc.)), 1h·1h. This signal is compensated by loss of signal from normal Auger final states, 2h (red area in the difference spectrum). For core-level excitations (**b**,**c**) such a clear distinction between local and non-local states is not possible because of the additional signal at similar kinetic energies that arises partially from participator Auger electrons (see text for details).

autoionization of light and heavy liquid water are shown in Fig. 2 for three different photon energies. In Fig. 2a the photon energy is 600 eV, which is sufficient to cause direct core ionization, being more than 60 eV above the O1*s* ionization threshold of liquid water[40]. The spectrum in Fig. 2a is dominated by normal Auger electron emission (Fig. 1b). For normal water, similar ionization–autoionization spectra were obtained previously[27,41,42]. Peak 1, near 505 eV KE, identifies the leading (normal) Auger transition. The feature relevant for the present study, however, is shoulder 2, near 510 eV KE. For core-level ionization (Fig. 2a), but not for excitation (see below), this peak has no gas-phase analogue[27] and is the unambiguous electronic-structure signature of 1h·1h final states, which have energies lower than those of the 2h states, and thus lead to a higher KE of the outgoing electron in the autoionization event. Our interpretation of the shoulder at 510 eV KE is supported further by our constrained density functional theory (DFT) calculations on small water clusters presented below and in Supplementary Figs S1 and S2.

The crucial observation to be made from Fig. 2a is, however, the much stronger intensity observed for 1h·1h states of $H_2O_{(aq)}$ as compared to those of $D_2O_{(aq)}$. Such a large isotope effect cannot result from the subtle ground-state structural differences between light and heavy water[43]. This agrees with the fact that the direct photoionization spectra of liquid water[44,45] and water clusters[46] exhibit a very small isotope effect, which is also consistent with our simulated Auger spectra being essentially identical for small water clusters formed by H_2O and D_2O when nuclear dynamic effects are not included (see Supplementary Figs S1 and S2). We therefore conclude that the difference spectrum of Fig. 2a reflects the effect of nuclear dynamics in the ionized state. The situation is different for excitation, when the extra electron must be taken into account. Absolute strengths of decay into 1h·1h states cannot be determined here because of the small intensity of peak 2 above the larger peak from local Auger decay, peak 1, the exact spectral shape of which is unknown.

Core-level excitation-induced autoionization spectra: $H_2O_{(aq)}$ versus $D_2O_{(aq)}$. For comparison we also present the analogous spectra for resonant excitations at the O1*s* absorption main-edge (537.5 eV photon energy (Fig. 2b)) and at the O1*s* absorption pre-edge (535 eV (Fig. 2c)). This case is considered only briefly here. In the excitation spectra, peak 1 appears at somewhat larger KEs because of spectator energy shifts, an effect previously discussed for water in great detail[41,42]. For core-level ionization and excitation the spectral changes between normal and deuterated water are fairly similar (compare the respective differential spectra). Proton dynamics thus seem to be of importance for decays from all intermediate states reached throughout the O1*s* near-edge absorption fine structure of liquid water (here the delocalized 2h final state contains an additional excited electron, 1e1h·1h). This was also concluded in previous X-ray emission studies[34–36,39]. In the present study, we used Auger spectroscopy for the experimental identification of nuclear dynamics on ionization, which is mediated by the solvent; gas-phase water does not dissociate on O1*s* ionization, but it does on excitation[30]. The dynamics of molecular water on core-level ionization and excitation were followed in detail by classical simulations[47]. These authors[47] corroborate the importance of O–H bond lengthening to explain the part of the spectrum designated as peak 2.

Nuclear motion in the core-ionized state. We now turn to a discussion concerning the nature of the 1h·1h states (peak 2 in Fig. 2a) in terms of PTM-CS processes (that is, steps 2′ and 3′ in Fig. 1d). To quantify the effects of nuclear dynamics we carried out calculations of proton dynamics in core-ionized water clusters.

Our results for the water dimer are shown in Fig. 3. The dimer geometry corresponds to the structure of condensed-phase water; here we use the I_h ice structure with the O···O distance set to 2.7 Å. Figure 3a shows the lowest potential energy curve along the O–H bonding direction of the core-ionized water molecule. This mode is identified as the most important proton-transfer coordinate

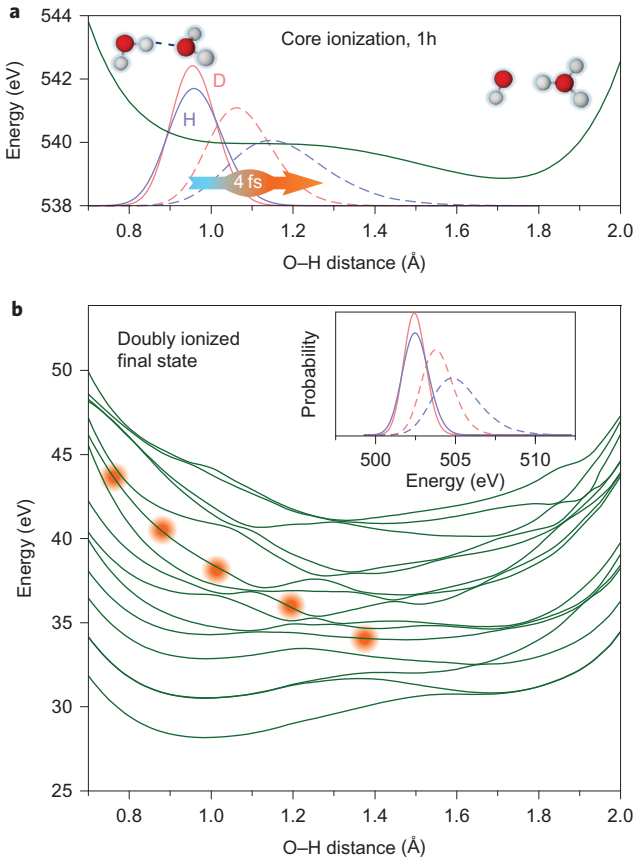

Figure 3 | Potential energy curves of ionized water dimers. a, Potential energy curve (green) along the hydrogen-transfer coordinate for the lowest core-ionized state of the water dimer from quantum dynamical calculations. Also shown are the respective wave packets (squared wave function) at times $t = 0$ fs (which corresponds to the ground-state molecular structure) and $t = 4$ fs (which corresponds to a Zundel-type intermediate). Wave packets for H_2O and D_2O are in blue and red, respectively; solid lines, $t = 0$ fs, and dashed lines, $t = 4$ fs. At the larger O–H distances to the far right, proton transfer is complete. **b**, Calculated energy curves of the doubly charged final states that result from autoionization of the cationic structures (**a**) evolving along the hydrogen-transfer coordinate. Large orange dots mark the lowest-energy 2h states and correspond to the doubly charged donor water unit (H_2O^{2+}···H_2O turning gradually into HO^+···H^+···H_2O); all the other states are of 1h·1h character (H_2O^+···H_2O^+ turning gradually into HO···H^+···H_2O^+). Only singlet electronic states are presented (triplet states are given in Supplementary Fig. S4). The inset shows kinetic energies of electrons that originate from local Auger process for light and heavy water for two different times; the positions of all the peaks are shifted to match the experimental maximum of the local Auger peak of normal water.

because the O–H bond vibrates rather fast, as does the free O–H bond, which, however, does not dissociate on core ionization. Potential energy curves for other relevant modes of the quasitetrahedral water pentamer are presented in Supplementary Fig. S3. In agreement with previous computations[39], we observed that for water clusters the O–H bond dissociation is energetically feasible, unlike that for gas-phase water ionization (see above). The electron-deficient core-ionized water molecule releases a proton to an accepting neighbouring water molecule (Fig. 1d, step 1). As the potential energy surface is rather flat, the driving force for this reaction is not strong. However, the energy content of the vibrational O–H wave packet is large and, as a consequence, the wave-packet dispersion is considerable even within the 4 fs core-hole lifetime. This is seen when the calculated wave packets of the ionized water dimer in the ground-state geometry are compared with the structure that evolves after 4 fs, when the average O–H distance has increased (Fig. 3a). Although the centre of the wave packet moves only slightly, there is a considerable change in shape, and the high-energy tail of the distribution quickly penetrates into the neighbouring molecule. Effects are smaller for heavy water with the distributions for D_2O staying much more compact. Note that the hydrogen-transfer process is barrierless for the O···O distances in liquid water, but a barrier does occur at larger distances[48,49].

These findings are in agreement with previous calculations[38,39]. Recent DFT-based simulations of core-ionized liquid water show that about 27% of water molecules have an O–H bond distance larger than 1.3 Å within the O1*s* lifetime[34,50]. At these elongated bond lengths, however, a proper distinction between the subunits in the $[HO^*\cdots H\cdots H_2O]^+$ hydrogen-bonded species is no longer possible (Fig. 1d).

The nature of the 1h·1h states. Figure 3b presents the singlet final-state energies of the doubly ionized water dimer along the hydrogen-transfer coordinate. These dicationic states are the final states of the autoionization process. The analysis of the electronic wavefunctions reveals that the nine lowest energies correspond to delocalized 1h·1h states. Near the ground-state geometry (that is, near an O–H distance of 1 Å), the lowest-energy delocalized states are the normal ICD states, $(1h\cdot1h)_{ICD}$; their electronic structure can be expressed as $H_2O^+\cdots H_2O^+$. The rates for decay into these states are probably rather small, as suggested by calculations for ammonia clusters[29], and normal ICD is unlikely to make a strong contribution to the 1h·1h peak in the spectrum. The first doubly ionized local state that corresponds to a $H_2O^{2+}\cdots H_2O$ charge distribution has, at the water equilibrium distance, an energy approximately 10 eV higher than that of the lowest delocalized state in the singlet manifold. This state, indicated by large orange dots in Fig. 3b, is essentially 2h in character; that is, the two positive charges can still be considered as localized on the initial water molecule. The large energy difference confirms that the 2h and $(1h\cdot1h)_{ICD}$ states can be distinguished readily by electron spectroscopy. For larger O–H/D distances, however, energies of the 2h state drop quickly. The electronic structure gradually changes from $H_2O^{2+}\cdots H_2O$ to $HO^+\cdots H^+\cdots H_2O$, denoted here as the $(1h\cdot1h)_{Auger}$ state.

The important conclusion from Fig. 3b is that PTM-Auger processes represent a viable route to populate the low-energy final dicationic states found in the experiment. For instance, at the O–H distance of 1.4 Å, the lowest-lying $(1h\cdot1h)_{Auger}$ final state (which has changed from a pure 2h state to approach a $(1h\cdot1h)_{Auger}$ state) is as much as 5 eV below the corresponding 2h energy in the ground-state geometry. We can only speculate as to the probability for the creation of 1h·1h states within an ICD-type transition (final state denoted as $(1h\cdot1h)_{ICD^*}$ with the electronic structure described best as $HO^+\cdots H^+ \cdots H_2O^+$). Arguably, these processes are favourable for larger O–H distances when the two water units interact more strongly. The energy difference between $(1h\cdot1h)_{Auger}$ and $(1h\cdot1h)_{ICD^*}$ states is, however, not large enough to distinguish these two types of PTM processes in the experiment. Internal conversion between $(1h\cdot1h)_{Auger}$ and $(1h\cdot1h)_{ICD^*}$ states, as indicated in Fig. 1d, is possible. Eventually the system undergoes further relaxation to the lowest level, but on a much slower timescale; a similar point was made by Ljungberg *et al.*[39]. The different PTM processes that lead to different charge-separated complexes probably affect the solution chemistry, but the details remain to be explored. Below we briefly speculate what happens after the autoionization event.

To make a more direct connection between the calculated energies of the 2h and 1h·1h states in Fig. 3b and the measured kinetic energies, the inset of Fig. 3b shows the projection of the

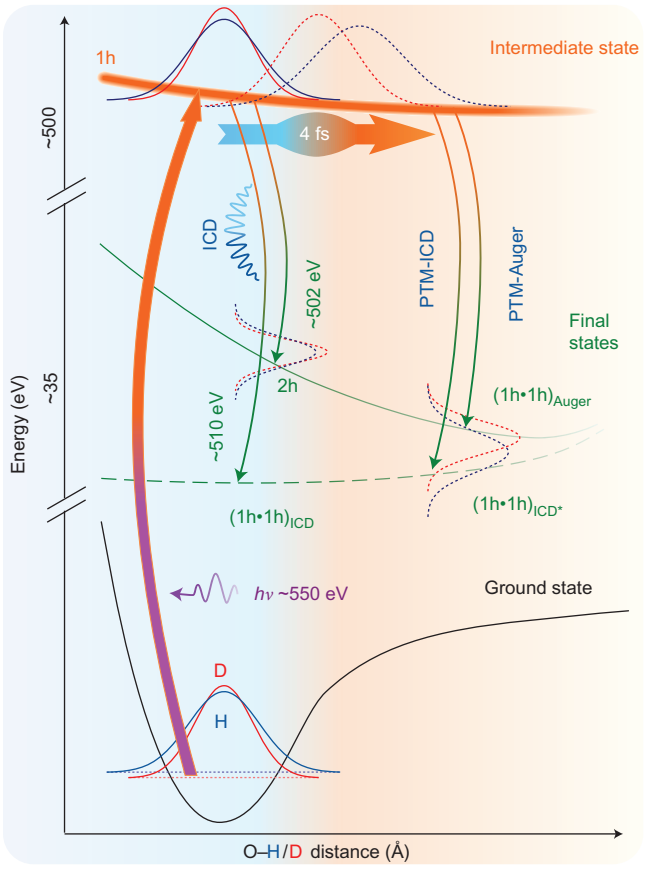

Figure 4 | The main findings of this work summarized in a graphical form. The potential energy curves of the ground state (black), core-ionized state (orange) and final states (green) are sketched. Photoionization projects the ground-state wave packets of normal and deuterated water (solid blue and red lines, respectively) onto the intermediate core-ionized state surface (thick orange arrow), which is repulsive along the proton-transfer coordinate (independent axis). Within 4 fs, the wave packets evolve, more so for normal water than deuterated (dotted blue and red lines, respectively). Within this time interval, autoionization occurs continuously (thin arrows, orange to green), and populates local 2h states and charge-separated states of the two different types discussed in the text, $(1h{\cdot}1h)_{ICD}$ and $(1h{\cdot}1h)_{Auger}$. The vertical Gaussians illustrate the distribution of energies of the doubly ionized states that are associated with autoionization of an evolving distribution of Zundel-like geometries.

wave packets from Fig. 3a on the energy axis, obtained by the reflection principle[46]. Results are shown only for the first singlet state (the singlet contribution typically dominates the overall spectral signal; triplet states are given in Supplementary Fig. S4), with the two holes localized on the hydrogen-donor molecule. We also restrict our analysis to $(1h{\cdot}1h)_{Auger}$ final states that correlate with the 2h state as these final states are formed within an essentially local autoionization process. The diabatic state that corresponds to the doubly charged donor water molecule is approximated by a linear function in the region spanned by the wave packet. The graphs thus represent the high-energy onsets of the Auger signal for the local Auger processes, blue for $H_2O_{(aq)}$ and red for $D_2O_{(aq)}$. Solid curves correspond to electron emission spectra from the initially populated structures, that is, for a wave packet at $t = 0$. Thus, the curve can be associated with the normal Auger signal of H_2O^{2+}. The dashed curves, shifted towards higher kinetic energies, represent electron emission that corresponds to the distribution of geometries the system would assume at 4 fs if no autoionization process took place. The final states then correspond to the $(1h{\cdot}1h)_{Auger}$ states. A further shift in energy is caused by populating $(1h{\cdot}1h)_{ICD^*}$ states, but it is not considered in the simulations in Fig. 3. As this shift is small, it was not resolved in the present experiment, and thus an experimental distinction between the two PTM-CS autoionization routes is not possible here. Regarding the decay probabilities, it seems reasonable that the probability of Auger decay of the core-excited Zundel-like cation is similar to that for Auger decay of a core-ionized single water molecule. Whether the PTM-ICD process becomes more probable than the normal ICD process is clearly one of the interesting questions that remain to be answered.

Indeed, analysis of the electronic structure in the core-ionized state supports the proton-transfer mechanism suggested above, whereas the transfer of a neutral hydrogen atom is less probable (for example, the partial charge on a transferred hydrogen at the O–H distance of 1.4 Å is 0.7e). The Mulliken population analysis and inspection of the electronic wavefunction also indicate that the electronic structure of the $(1h{\cdot}1h)_{Auger}$ and $(1h{\cdot}1h)_{ICD^*}$ final states can, indeed, be associated with $HO^+{\cdots}H^+{\cdots}H_2O$ and $HO^+{\cdots}H^+{\cdots}H_2O^+$. Such a description is, however, only approximate because of the strong interaction between the moieties. Although the above structures represent the dominant 'resonance structures', one can also expect a certain degree of covalency.

Implications for radiation chemistry. It follows from our arguments that the core ionization of liquid water leads not only to the formation of the doubly charged H_2O^{2+} molecule, but also to charge-separated $[OH^+{\cdots}H_3O^+]_{(aq)}$ and $[H_2O^+{\cdots}H_2O^+]_{(aq)}$ complexes formed in highly excited vibrational states. The possible role of the $[H_2O^+{\cdots}H_2O^+]_{(aq)}$ complex formed within the regular ICD for biomolecular damage was discussed recently[21,51]. However, so far neither the PTM-ICD-type nor the Auger-type charge-separated states have been considered. We can only speculate on the reactions that follow the autoionization process, and we argue that even the relatively subtle differences in energy and structure for ICD versus PTM-ICD will have an effect on the subsequent chemical reactions. After formation of the doubly charged system, the two positive charges created in close proximity will be forced to separate because of the strong Coulombic repulsion. Very probably the charge separation proceeds via release of protons towards neighbouring water molecules; proton transfer between H_2O^+ and H_2O is very fast for a valence-ionized water molecule (~20 fs)[52] and the gas-phase rate constant for the reaction of OH^+ with water is almost as large as that for the $H_2O^+ + H_2O$ reaction[53]. Thus, two OH radicals and two H_3O^+ cations are probably formed immediately, starting from $[H_2O^+{\cdots}H_2O^+]_{(aq)}$, and an oxygen atom and two H_3O^+ cations or an OH radical and another H_2O^+ will result from $[OH^+{\cdots}H_3O^+]_{(aq)}$ species[53]. On a longer (subpicosecond) scale, the overall result of the core ionization is the formation of various reactive oxygen species, particularly OH radicals, $O(^3P)$ atoms and H_2O_2; similar processes are considered for multiple ionization in water radiolysis[9]. The relative yield, spatial distribution and energy state of these reactive particles are controlled by the early processes described herein.

Conclusions

We have identified experimentally a novel type of non-radiative relaxation process on core ionization in a hydrogen-bonded system. These processes lead to new types of dicationic charge-separated species, $[OH^+{\cdots}H_3O^+]_{(aq)}$ and $[H_2O^+{\cdots}H_2O^+]_{(aq)}$, that form on the core ionization of liquid water and involves ultrafast dissociative nuclear motion. Until now these species were not accounted for in the radiation chemistry of water, which usually assumes $H_2O^{2+}_{(aq)}$ as the only doubly charged species created initially. In particular, Auger processes, other than the

local one, have yet to be considered in water radiation chemistry and physics[2,54,55].

Figure 4 summarizes graphically our main findings. Within a few femtoseconds, core ionization of liquid water leads to a time-evolving cationic Zundel-type structure that contains a bridging proton and a core-excited HO* radical, which then autoionizes. Energies of this transient cationic structure are shown at the top Fig. 4, and the two PTM-CS autoionization channels, one local (PTM-Auger) and one non-local (PTM-ICD), are depicted. The final charge-separated reactive dicationic products of the PTM routes have much lower energies than the doubly charged water molecule, H_2O^{2+}, and hence the charge-delocalized complexes probably play different roles in radiation-induced processes in water. The two charge-separated forms, $[OH^+\cdots H_3O^+]_{(aq)}$ (from PTM-Auger) and $[H_2O^+\cdots H_2O^+]_{(aq)}$ (from PTM-ICD), engage in different immediate fragmentations that probably lead to different spatial and internal energy distributions in the primary products, and thus, in turn, to different contributions to the overall radical yields going on to the diffusive phase of the radiation chemistry. In contrast to valence ionization, PTM processes tend to lead to more radical centres, and the damage yield is thus higher. Analogous relaxation processes that involve proton transfer and autoionization seem, so far, to be exclusive for processes initiated by core ionization. The autoionization processes are closed energetically on outer-valence ionization. For inner-valence ionization of the water dimer, the ICD channel is open, but sequential double ionization by PTM autoionization has not been identified[56].

We argue that simulations of radiation chemistry processes at the molecular level need to include the mechanisms identified here. Furthermore, we expect that the PTM-Auger and PTM-ICD processes represent a generic feature for hydrogen-bonded systems. Recent advances in X-ray science, such as the advent of ultrashort pulses from free-electron lasers and high harmonics sources, may allow us to further detail the findings in this work by time-resolved experiments.

Methods

Experimental. Photoelectron-spectroscopy measurements were performed from a 15 μm vacuum liquid-water jet[57,58] at the soft-X-ray U41-PGM undulator beamline of BESSY II, Berlin. The jet velocity was ~80 ms^{-1} and the jet temperature was 6 °C. Electrons were detected with a hemispherical electron analyser, separated from the liquid jet by a 100 μm diameter orifice at a distance of approximately 0.3 mm. Details regarding jet preparation, experimental resolution and spectra acquisition are described elsewhere[57,59].

Computational. The calculations of dynamical events following the core ionization were performed on a water dimer model with geometrical parameters taken from hexagonal ice, setting the O···O distance exactly to 2.7 Å. The core-ionized states were calculated using the complete active space self-consistent field (CASSCF) method with frozen core orbitals. We used an active space that consisted of 19 electrons in ten molecular orbitals. The doubly ionized states were calculated with the CASSCF method, with an active space of ten electrons in seven orbitals. States with singlet multiplicity were considered (triplet states shown in the Supplementary Fig. S4). The character of the final states (localized or delocalized positive charge) was analysed by expressing the configuration state functions in a basis of localized molecular orbitals. The energies of Auger electrons for a given structure were calculated as a difference between the water dimer of the core-ionized species and the doubly charged species. The probability of an Auger-type transition was considered to be independent of the O–H distance, considering the final states with localized charge on the initial core-hole atom only. The aug-cc-pCVDZ basis was used for oxygen and aug-cc-pVDZ basis for hydrogen. All calculations were done with MOLPRO 2009 suites of codes[60].

The nuclear wavefunction was propagated on the core-ionized potential energy surface using a split operator technique. The wave packet was discretized on 1,024 grid points on a grid that ranged from 0.6 to 2.2 Å with an imaginary absorption potential applied on the boundaries. A time step of one arbitrary unit was used in the propagation. The initial wavefunction was obtained by wave-packet propagation in imaginary time.

Received 23 November 2012; accepted 3 May 2013;
published online 20 June 2013

References

1. Seiwert, T. Y., Salama, J. K. & Vokes, E. E. The concurrent chemoradiation paradigm – general principles. *Nature Clin. Pract. Oncol.* **4,** 86–100 (2007).
2. Howell, R. W. Auger processes in the 21st century. *Int. J. Radiat. Biol.* **84,** 959–975 (2008).
3. Eschenbrenner, A. *et al.* Strand breaks induced in plasmid DNA by ultrasoft X-rays: influence of hydration and packing. *Int. J. Radiat. Biol.* **83,** 687–697 (2007).
4. Wang, C. R., Nguyen, J. & Lu, Q. B. Bond breaks of nucleotides by dissociative electron transfer of nonequilibrium prehydrated electrons: a new molecular mechanism for reductive DNA damage. *J. Am. Chem. Soc.* **131,** 11320–11322 (2009).
5. Alizadeh, E. & Sanche, L. Precursors of solvated electrons in radiobiological physics and chemistry. *Chem. Rev.* **112,** 5578–5602 (2012).
6. Weik, M. *et al.* Specific chemical and structural damage to proteins produced by synchrotron radiation. *Proc. Natl Acad. Sci. USA* **97,** 623–628 (2000).
7. Hatano, Y., Katsumura, Y. & Mozumder, A. *Charged Particle and Photon Interactions with Matter: Recent Advances, Applications, and Interfaces* (CRC Press, 2010).
8. Garrett, B. C. *et al.* Role of water in electron-initiated processes and radical chemistry: issues and scientific advances. *Chem. Rev.* **105,** 355–389 (2005).
9. Meesungnoen, J. *et al.* Multiple ionization effects on the yields of HO_2/O_2^- and H_2O_2 produced in the radiolysis of liquid water with high-LET $^{12}C^{6+}$ ions: a Monte-Carlo simulation study. *Chem. Phys. Lett.* **377,** 419–425 (2003).
10. Tavernelli, I. *et al.* Time-dependent density functional theory molecular dynamics simulations of liquid water radiolysis. *Chem. Phys. Chem.* **9,** 2099–2103 (2008).
11. Gaigeot, M. P. *et al.* A multi-scale *ab initio* theoretical study of the production of free radicals in swift ion tracks in liquid water. *J. Phys. B* **40,** 1–12 (2007).
12. Cederbaum, L. S., Zobeley, J. & Tarantelli, F. Giant intermolecular decay and fragmentation of clusters. *Phys. Rev. Lett.* **79,** 4778–4781 (1997).
13. Müller, I. B. & Cederbaum, L. S. Electronic decay following ionization of aqueous Li^+ microsolvation clusters. *J. Chem. Phys.* **122,** 194305 (2005).
14. Hergenhahn, U. Interatomic and intermolecular Coulombic decay: the early years. *J. Electron Spectrosc. Relat. Phenom.* **184,** 78–90 (2011).
15. Marburger, S., Kugeler, O., Hergenhahn, U. & Möller, T. Experimental evidence for interatomic Coulombic decay in Ne clusters. *Phys. Rev. Lett.* **90,** 203401 (2003).
16. Jahnke, T. *et al.* Experimental observation of interatomic Coulombic decay in neon dimers. *Phys. Rev. Lett.* **93,** 163401 (2004).
17. Hergenhahn, U. Production of low kinetic energy electrons and energetic ion pairs by intermolecular Coulombic decay. *Int. J. Radiat. Biol.* **88,** 871–883 (2012).
18. Mucke, M. *et al.* A hitherto unrecognized source of low-energy electrons in water. *Nature Phys.* **6,** 78–81 (2010).
19. Schwartz, C. P., Fatehi, S., Saykally, R. J. & Prendergast, D. Importance of electronic relaxation for inter-Coulombic decay in aqueous systems. *Phys. Rev. Lett.* **105,** 198102 (2010).
20. Lindblad, A. *et al.* Charge delocalization dynamics of ammonia in different hydrogen bonding environments: free clusters and in liquid water solution. *Phys. Chem. Chem. Phys.* **11,** 1758–1764 (2009).
21. Stoychev, S. D., Kuleff, A. I. & Cederbaum, L. S. Intermolecular Coulombic decay in small biochemically relevant hydrogen-bonded systems. *J. Am. Chem. Soc.* **133,** 6817–6824 (2011).
22. Aziz, E. F., Ottosson, N., Faubel, M., Hertel, I. V. & Winter, B. Interaction between liquid water and hydroxide revealed by core-hole de-excitation. *Nature* **455,** 89–91 (2008).
23. Pokapanich, W. *et al.* Auger electron spectroscopy as a probe of the solution of aqueous ions. *J. Am. Chem. Soc.* **131,** 7264–7271 (2009).
24. Pokapanich, W. *et al.* Ionic-charge dependence of tie intermolecular Coulombic decay time scale for aqueous ions probed by the core-hole clock. *J. Am. Chem. Soc.* **133,** 13430–13436 (2011).
25. Pokapanich, W. *et al.* Bond breaking, electron pushing, and proton pulling: active and passive roles in the interaction between aqueous ions and water as manifested in the O1*s* Auger decay. *J. Phys. Chem. B* **116,** 3–8 (2012).
26. Ottosson, N., Öhrwall, G. & Björneholm, O. Ultrafast charge delocalization dynamics in aqueous electrolytes: new insights from Auger electron spectroscopy. *Chem. Phys. Lett.* **543,** 1–11 (2012).
27. Öhrwall, G. *et al.* The electronic structure of free water clusters probed by Auger electron spectroscopy. *J. Chem. Phys.* **123,** 054310 (2005).
28. Stoychev, S. D., Kuleff, A. I. & Cederbaum, L. S. On the intermolecular Coulombic decay of singly and doubly ionized states of water dimer. *J. Chem. Phys.* **133,** 154307 (2010).
29. Kryzhevoi, N. V. & Cederbaum, L. S. Non local effects in the core ionization and Auger spectra of small ammonia clusters. *J. Phys. Chem. B* **115,** 5441–5447 (2011).
30. Hjelte, I. *et al.* Evidence for ultra-fast dissociation of molecular water from resonant Auger spectroscopy. *Chem. Phys. Lett.* **334,** 151–158 (2001).

31. Björneholm, O., Nilsson, A., Sandell, A., Hernnas, B. & Martensson, N. Determination of time scales for charge-transfer screening in physisorbed molecules. *Phys. Rev. Lett.* **68,** 1892–1895 (1992).
32. Schnadt, J. *et al.* Experimental evidence for sub-3-fs charge transfer from an aromatic adsorbate to a semiconductor. *Nature* **418,** 620–623 (2002).
33. Föhlisch, A. *et al.* Direct observation of electron dynamics in the attosecond domain. *Nature* **436,** 373–376 (2005).
34. Odelius, M. *et al.* Ultrafast core-hole-induced dynamics in water probed by X-ray emission spectroscopy. *Phys. Rev. Lett.* **94,** 227401 (2005).
35. Fuchs, O. *et al.* Isotope and temperature effects in liquid water probed by X-ray absorption and resonant X-ray emission spectroscopy. *Phys. Rev. Lett.* **100,** 027801 (2008).
36. Tokushima, T. *et al.* High resolution X-ray emission spectroscopy of liquid water: the observation of two structural motifs. *Chem. Phys. Lett.* **460,** 387–400 (2008).
37. Odelius, M. Molecular dynamics simulations of fine structure in oxygen K-edge X-ray emission spectra of liquid water and ice. *Phys. Rev. B* **79,** 144204 (2009).
38. Ljungberg, M. P., Nilsson, A. & Pettersson, L. G. M. Semiclassical description of nuclear dynamics in X-ray emission of water. *Phys. Rev. B* **82,** 245115 (2010).
39. Ljungberg, M. P., Pettersson, L. G. M. & Nilsson, A. Vibrational interference effects in X-ray emission of a model water dimer: implications for the interpretation of the liquid spectrum. *J. Chem. Phys.* **134,** 044513 (2011).
40. Winter, B., Aziz, E. F., Hergenhahn, U., Faubel, M. & Hertel, I. V. Hydrogen bonds in liquid water studied by photoelectron spectroscopy. *J. Chem. Phys.* **126,** 124504 (2007).
41. Winter, B., Hergenhahn, U., Faubel, M., Björneholm, O. & Hertel, I. V. Hydrogen bonding in liquid water probed by resonant Auger-electron spectroscopy. *J. Chem. Phys.* **127,** 094501 (2007).
42. Nordlund, D. *et al.* Probing the electron delocalization in liquid water and ice at attosecond time scales. *Phys. Rev. Lett.* **99,** 217406 (2007).
43. Soper, A. K. & Benmore, C. J. Quantum differences between heavy and light water. *Phys. Rev. Lett.* **101,** 065502 (2008).
44. Winter, B. *et al.* Full valence band photoemission from liquid water using EUV synchrotron radiation. *J. Phys. Chem. A* **108,** 2625–2632 (2004).
45. Nishizawa, K. *et al.* High-resolution soft X-ray photoelectron spectroscopy of liquid water. *Phys. Chem. Chem. Phys.* **13,** 413–417 (2011).
46. Barth, S. *et al.* Valence ionization of water clusters: from isolated molecules to bulk. *J. Phys. Chem. A* **113,** 13519–13527 (2009).
47. Takahashi, O. *et al.* Auger decay calculations with core-hole excited-state molecular-dynamics simulations of water. *J. Chem. Phys.* **124,** 064307 (2006).
48. Felicissimo, V. C., Guimaraes, F. F., Gel'mukhanov, F., Cesar, A. & Ågren, H. The principles of infrared-X-ray pump-probe spectroscopy. Applications on proton transfer in core-ionized water dimers. *J. Chem. Phys.* **122,** 094319 (2005).
49. Felicissimo, V. C. *et al.* A theoretical study of the role of the hydrogen bond on core ionization of the water dimer. *Chem. Phys.* **312,** 311–318 (2005).
50. Stia, C. R. *et al.* Theoretical investigation of the ultrafast dissociation of core-ionized water and uracil molecules immersed in liquid water. *Eur. Phys. J. D* **60,** 77–83 (2010).
51. Vendrell, O., Stoychev, S. D. & Cederbaum, L. S. Generation of highly damaging H_2O^+ radicals by inner valence shell ionization of water. *Chem. Phys. Chem.* **11,** 1006–1009 (2010).
52. Marsalek, O. *et al.* Chasing charge localization and chemical reactivity following photoionization in liquid water. *J. Chem. Phys.* **135,** 224510 (2011).
53. Anicich, V. G. Evaluated biomolecular ion-molecule gas-phase kinetics of positive ion for use in modeling planetary atmosphere, cometary comae, and interstellar clouds. *J. Phys. Chem. Ref. Data* **22,** 1469–1569 (1993).
54. Pimblott, S. M. & LaVerne, J. A. Stochastic simulation of the electron radiolysis of water and aqueous solutions. *J. Phys. Chem. A* **101,** 5828–5838 (1997).
55. Garrett, B. C. Ions at the air/water interface. *Science* **303,** 1146–1147 (2004).
56. Jahnke, T. *et al.* Ultrafast energy transfer between water molecules. *Nature Phys.* **6,** 139–142 (2010).
57. Winter, B. & Faubel, M. Photoemission from liquid aqueous solutions. *Chem. Rev.* **106,** 1176–1211 (2006).
58. Winter, B. Liquid microjet for photoelectron spectroscopy. *Nucl. Instrum. Meth. A* **601,** 139–150 (2009).
59. Seidel, R., Thürmer, S. & Winter, B. Photoelectron spectroscopy meets aqueous solution: studies from a vacuum liquid microjet. *J. Phys. Chem. Lett.* **2,** 633–641 (2011).
60. MOLPRO, version 2010.1. A package of *ab initio* programs (University College, Cardiff, 2010).

Acknowledgements

We thank N. Kryzhevoi and L. S. Cederbaum for stimulating discussions. We acknowledge the support of the Grant agency of the Czech Republic via grants no. P208/10/1724 and P208/11/0161 to P.S., the US National Science Foundation (CHE-0957869) to S.E.B., the Deutsche Forschungsgemeinschaft (DFG) via projects WI 1327/3-1, UH 3060/5-1, and the DFG Research Unit FOR 1789.

Author contributions

S.T. and B.W. conceived, designed and performed the experiments, and analysed the data. P.S. and M.O. conducted the calculations and contributed to data interpretation. N.O. and R.S. contributed materials and/or analysis tools. B.W., P.S., S.T., U.H. and S.E.B. co-wrote the paper. All authors discussed the results and commented on the manuscript.

Additional information

Supplementary information is available in the online version of the paper. Reprints and permissions information is available online at www.nature.com/reprints. Correspondence and requests for materials should be addressed to P.S. and B.W.

Competing financial interests

The authors declare no competing financial interests.